Ryder et al, Figure S1

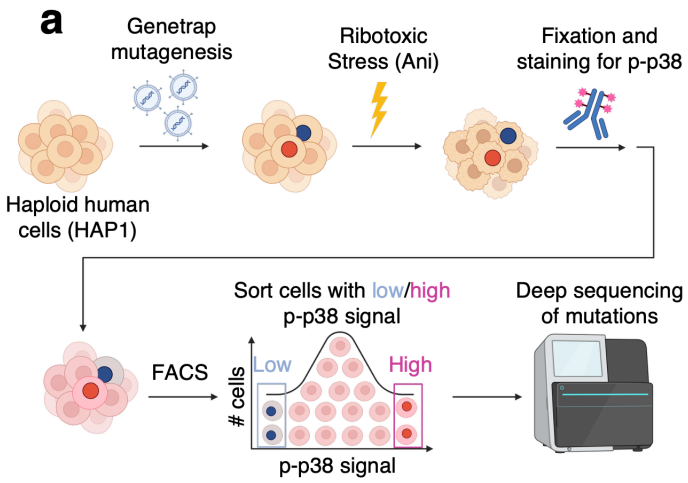

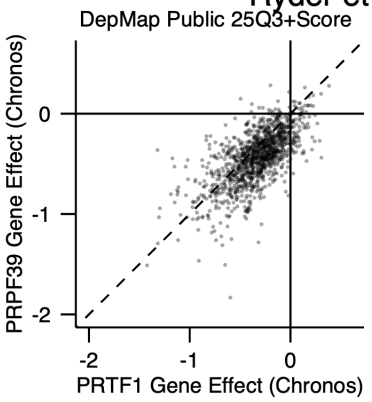

***PRPF39* top co-dependencies**

Gene	Pearson correlation
PRTF1	0.66
JRK	0.45
IL3RA	0.44
FBRS	-0.42
UBE2L5	-0.41

***PRTF1* top co-dependencies**

Gene	Pearson correlation
PRPF39	0.66
SLC35G4	-0.53
SMIM32	-0.44
SHOX	-0.40
MAGEL2	-0.38

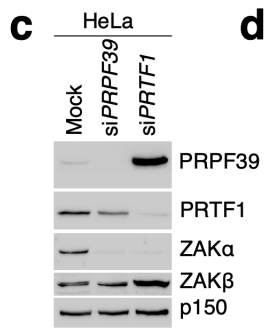

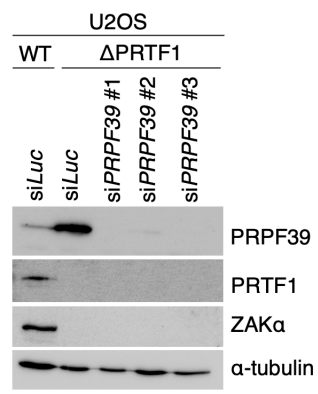

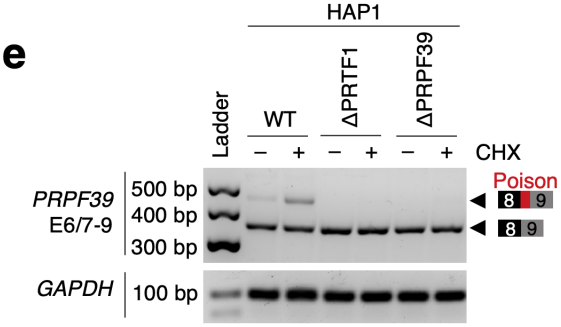

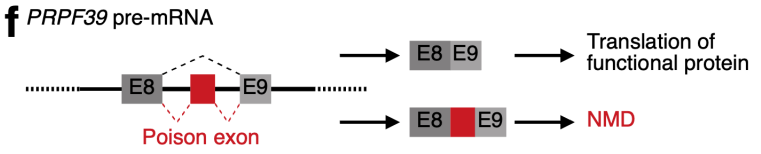

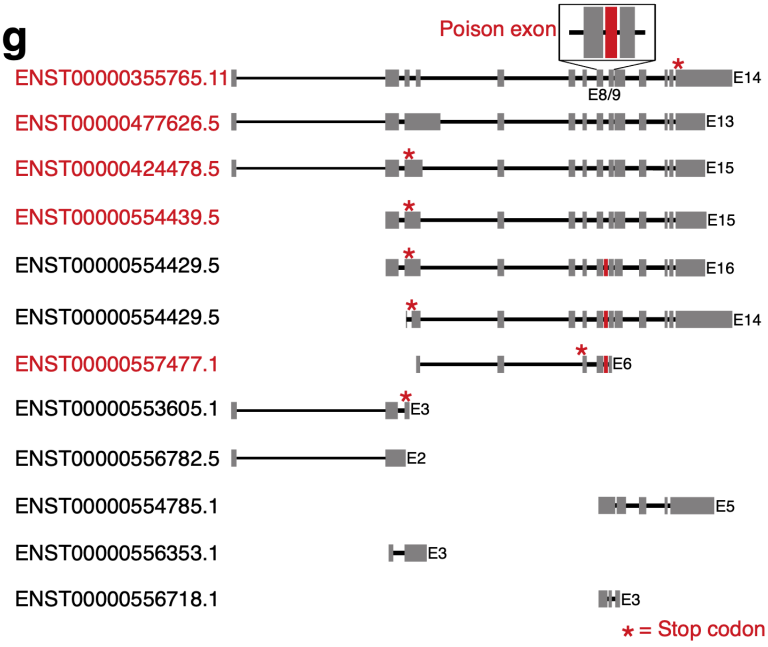

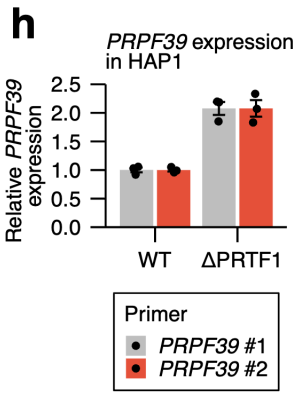

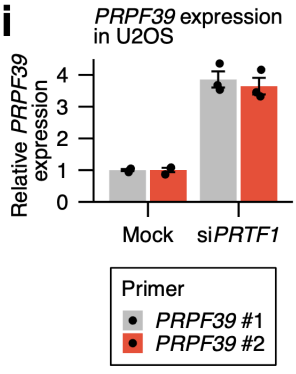

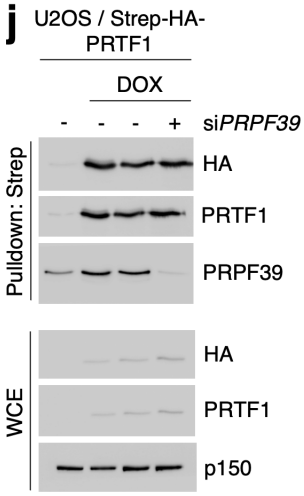

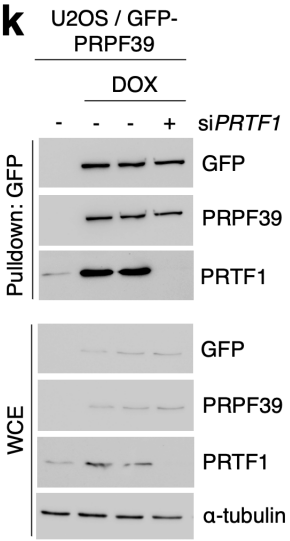

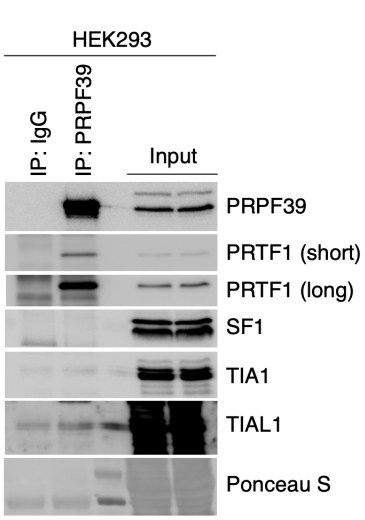

Figure S1.

Co-dependency, co-expression and interaction between PRPF39 and PRTF1

a. Schematic of the haploid genetic screen workflow to map genetic regulators of p38 activation in response to anisomycin. **b.** Co-dependency of PRPF39 and PRTF1 (TRNAU1AP) for growth across a panel of CRISPR-screened cancer cell lines. Data were harvested from the DepMap resource (depmag.org). **c.** HeLa cells were transfected with siRNAs targeting PRPF39 and PRTF1 for 72 h. Lysates were analyzed by immunoblotting with the indicated antibodies. **d.** WT U2OS and ΔPRTF1 cells were transfected with PRPF39-targeting siRNAs as indicated (72 h). Lysates were analyzed as in (c). **e.** RNA extracted from HAP1 cells with the indicated genotypes was reverse-transcribed, and the resulting DNA was analyzed by PCR with primers annealing to exons upstream and downstream of *PRPF39* poison exon. Cells were pre-treated with cycloheximide (100 μg/ml, 2 h) when indicated to assay for nonsense mediated decay (NMD) of exon-skipped splice forms. **f.** Schematic of poison exon inclusion and NMD of the *PRPF39* transcript. **g.** Annotated splice forms of the *PRPF39* transcript (gtexportal.org). The position of the known poison exon between exons 8 and 9 is indicated. Additional poison exons are located between exons 3 and 4. **h.** qPCR-based analysis of spliced *PRPF39* transcript levels in WT HAP1 and ΔPRTF1 cells. Two independent primer pairs were used. **i.** As in (h), except that PRTF1 siRNA-transfected U2OS cells were used. **j.** U2OS cells stably transfected with doxycycline (DOX)-inducible Strep-HA-PRTF1 were treated with PRPF39 siRNA (72h) as indicated and subjected to strep purification. Pulldown material and whole cell extract (WCE) were analyzed as in (c). **k.** U2OS cells stably transfected with doxycycline (DOX)-inducible GFP-PRPF39 were treated with PRTF1 siRNA (72h) as indicated and subjected to GFP purification. Pulldown material and WCE were analyzed as in (c). **l.** U2OS cell lysates were subjected to immunoprecipitation (IP) with PRPF39 antibodies or IgG control.

IP’ed material and WCE was analyzed as in (c). (h, i) Data are plotted as mean and all error bars represent the standard deviation (SD) (n=3 biological replicates).

Ryder et al, Figure S2

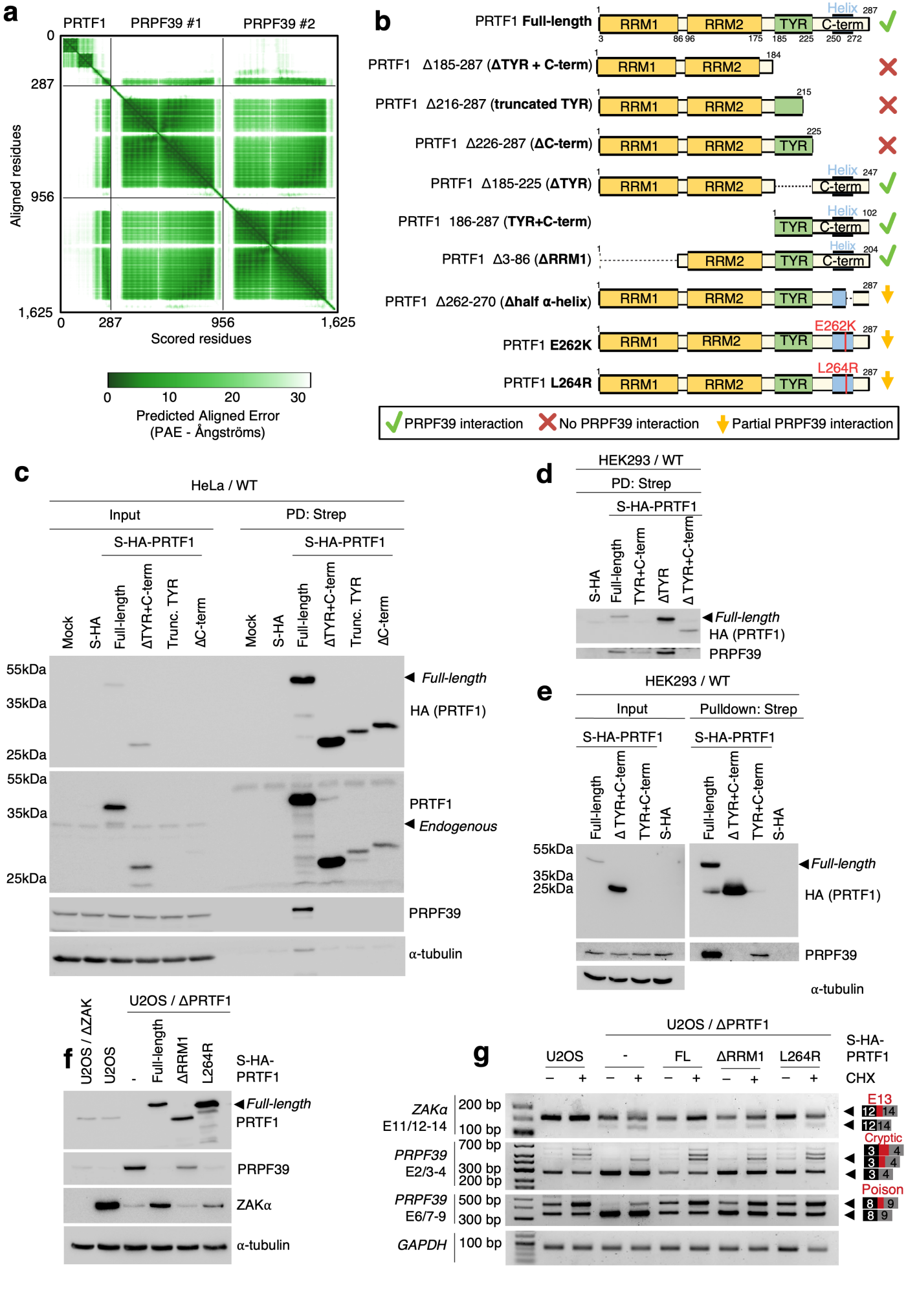

Figure S2.

Elucidation of a functional PRPF39-PRTF1 complex by Alphafold modelling and mutagenesis.

a. Predicted aligned error (PAE) matrix plot of an Alphafold 3-generated prediction of a PRPF39-PRPF39-PRTF1 complex. **b.** Schematic of deletion and point mutants of PRTF1 generated in this study. Effect of mutation on PRPF39 is indicated (green, no effect; red, loss of interaction; yellow, decreased interaction). **c.** HeLa cells were transfected with the indicated WT and mutant constructs of strep-HA-PRTF1. Lysates were subjected to strep purification and pulldown material and WCE were analyzed by immunoblotting with the indicated antibodies. **d.** As in (c), except that HEK293 cells were used. **e.** As in (c) and (d) but with transfection of the indicated PRTF1 constructs. **f.** U2OS ΔPRFT1 cells were stably rescued with the indicated versions of strep-HA-tagged PRTF1 constructs. Lysates were analyzed as in (c). **g.** RNA extracted from cell lines from (f) was reverse-transcribed, and the resulting DNA was analyzed by PCR with primers annealing to exons 12 and 14 of *ZAK*α, exons 3 and 4 of *PRPF39* and exons 8 and 9 of *PRPF39*, respectively. Cells were pre-treated with cycloheximide (100 μg/ml, 2 h) when indicated to assay for NMD of exon-skipped splice forms. Reactions were separated and analyzed by agarose gel electrophoresis.

Ryder et al, Figure S3

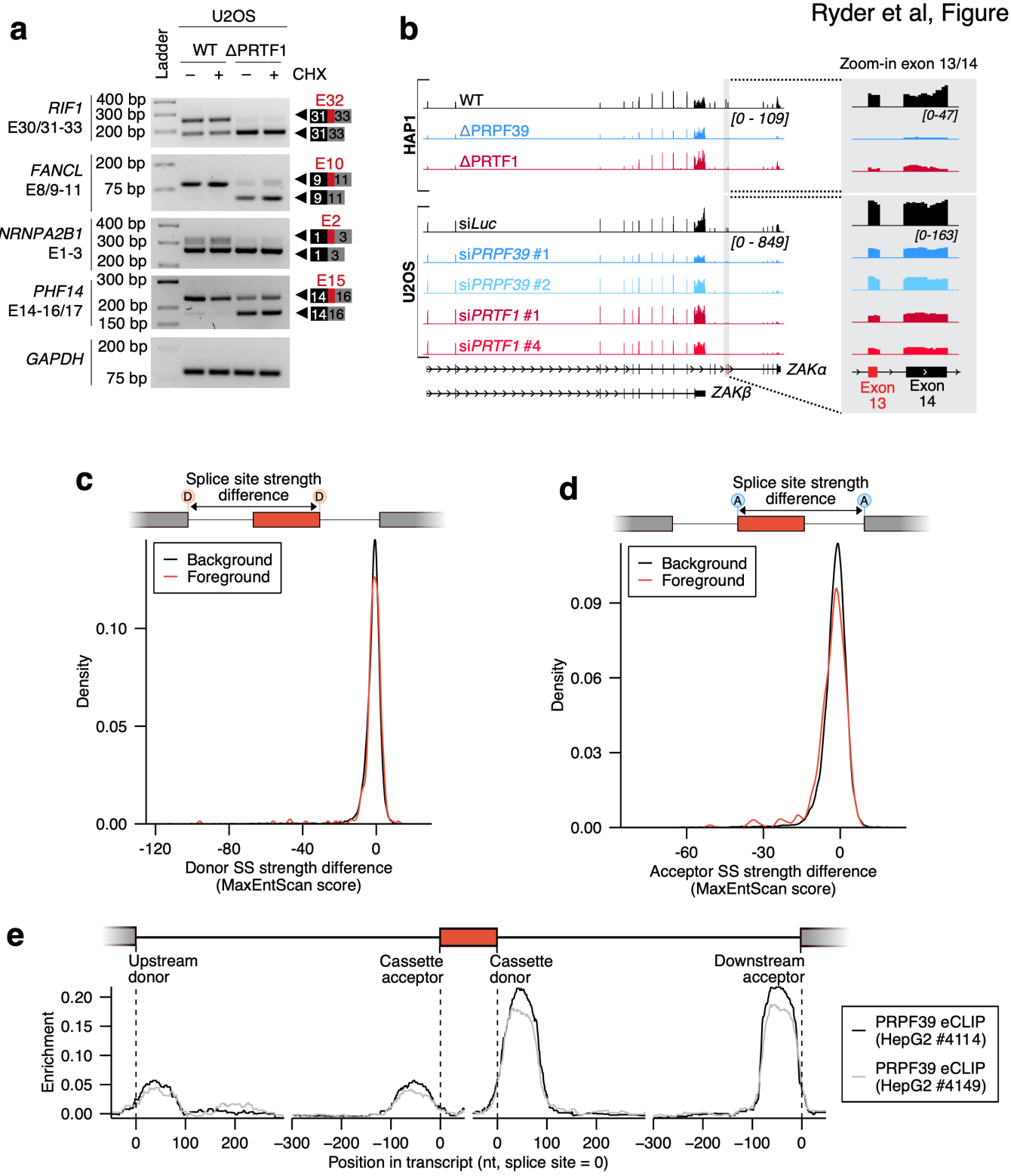

Figure S3.

Splicing phenotypes are independent of consensus splice-site sequence strength

a. RNA extracted from U2OS WT and ΔPRTF1 cells was reverse-transcribed, and the resulting DNA was analyzed by PCR primers annealing to the indicated exons. Cells were pre-treated with cycloheximide (100 μg/ml, 2 h) when indicated to assay for nonsense mediated decay (NMD) of exon-skipped splice forms. Reactions were separated and analyzed by agarose gel electrophoresis. **b.** RNA sequencing read tracks from all sequencing reactions across *MAP3K20*/*ZAK* mRNA. Blow-up highlights both the decrease in signal from skipped exon 13 of *ZAKα* and loss of downstream exons due to NMD. **c.** Relative donor splice-site (5' SS) strength computed by MaxEntScan for human foreground and background exons (datasets from Fig. 2l). Density distributions are plotted as functions of the difference to the competing upstream donor. **d.** As in (c), except that the difference between competing acceptor scores is plotted. **e.** Metagene plot of PRPF39 eCLIP signal enrichment (foreground events over background events from Fig. 2l) across cassette exons and upstream and downstream introns. Enrichment distributions are plotted in windows of 300 nt downstream of donor sites and upstream of acceptor sites, respectively (data from RBP-ARK for two PRPF39 antibodies in HepG2 cells are shown).

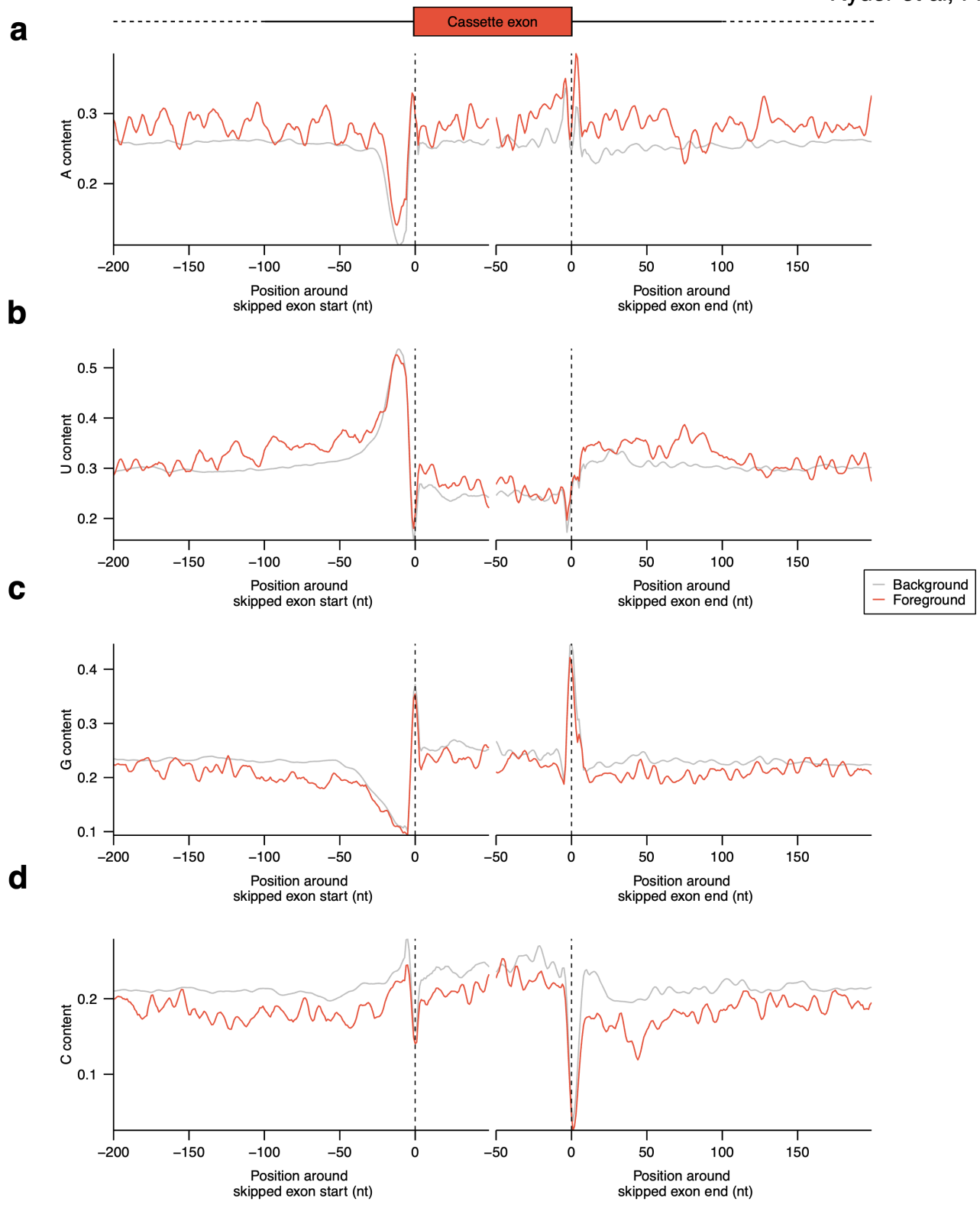
a
Cassette exon
A content
0.3
0.2
−200 −150 −100 −50 0
−50 0 50 100 150
Position around skipped exon start (nt)
Position around skipped exon end (nt)
b
U content
0.5
0.4
0.3
0.2
c
G content
0.4
0.3
0.2
0.1
d
C content
0.2
0.1
Background
Foreground

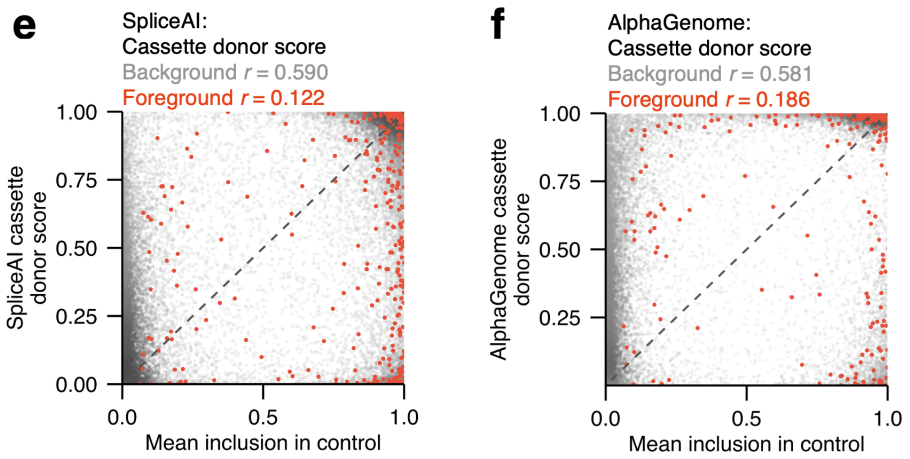
e
SpliceAI:
Cassette donor score
Background r = 0.590
Foreground r = 0.122
SpliceAI cassette donor score
1.00
0.75
0.50
0.25
0.00
0.0 0.5 1.0
Mean inclusion in control
f
AlphaGenome:
Cassette donor score
Background r = 0.581
Foreground r = 0.186
AlphaGenome cassette donor score
1.00
0.75
0.50
0.25
0.0 0.5 1.0
Mean inclusion in control

Figure S4.

Nucleotide composition biases in mRNA regions encompassing PRPF39-PRTF1-dependent exons

a. Metagene plot highlighting A content across cassette exons and adjacent sequences in foreground compared to background datasets. Dashed lines indicate 5' (acceptor) and 3' SS (donor) of the cassette exon, respectively. **b.** As in (a), except for U content. **c.** As in (a), except for G content. **d.** As in (a), except for C content. **e.** SpliceAI-computed cassette donor splice-site scores plotted against experimentally derived exon inclusion levels in the control conditions and color-coded according to presence in human foreground (red) and background (grey) datasets (data from Fig. 2l). Performance comparison (Pearson *r*) is indicated for the two classes. **f.** As in (e) but with AlphaGenome-computed cassette donor splice-site scores.

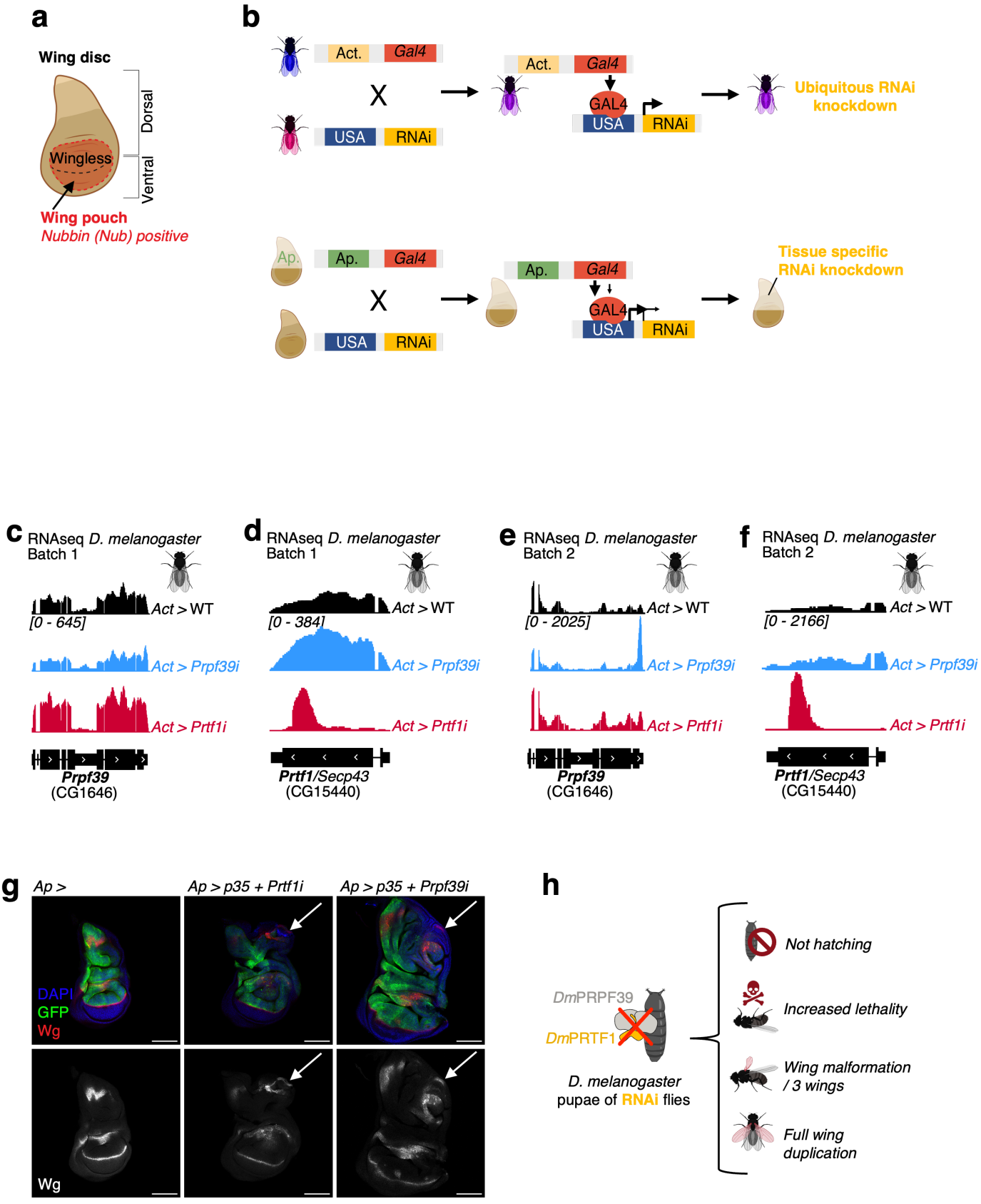
a
Wing disc
Dorsal
Ventral
Wingless
Wing pouch
Nubbin (Nub) positive
b
Act.
Gal4
X
USA
RNAi
GAL4
Ubiquitous RNAi knockdown
Ap.
Tissue specific RNAi knockdown
c
RNAseq D. melanogaster Batch 1
Act > WT
[0 - 645]
Act > Prpf39i
Act > Prtf1i
Prpf39 (CG1646)
d
RNAseq D. melanogaster Batch 1
[0 - 384]
Prtf1/Secp43 (CG15440)
e
RNAseq D. melanogaster Batch 2
[0 - 2025]
f
RNAseq D. melanogaster Batch 2
[0 - 2166]
g
Ap >
Ap > p35 + Prtf1i
Ap > p35 + Prpf39i
DAPI
GFP
Wg
h
DmPRPF39
DmPRTF1
D. melanogaster pupae of RNAi flies
Not hatching
Increased lethality
Wing malformation / 3 wings
Full wing duplication

Figure S5.

Wing duplication phenotype of *DmPrpf39*/*DmPrtf1* RNAi-expressing flies

a. Anatomy of the wing imaginal disc and **b.** genetic strategies employed to knockdown and express proteins in *Drosophila melanogaster*. Ubiquitous depletion was achieved by crossing UAS lines encoding the RNAi of interest with the Actin-Gal4 line. Knockdown in the dorsal compartment of the wing imaginal disc was achieved by crossing with Ap-Gal4. Apoptosis induction was further blocked by introducing p35 transgenic flies into these crosses. **c.-f.** Averaged RNA sequencing read tracks across the *DmPrpf39* (c, e) and *DmPrtf1* (d,f) transcripts in experiments from Fig. 6b. **g.** Fly larvae expressing apoptosis-blocking p35 protein and *DmPrtf1* RNAi or *DmPrpf39* RNAi in the dorsal wing imaginal disc compartment (under control of Ap-Gal4 driver - GFP marker) were immunostained with antibodies against the morphogen Wingless (Wg) and counterstained for DNA content with DAPI. Arrows indicate areas with ectopic Wingless expression. Scale bars = 100 μm. **h.** Overview of overlapping phenotypes associated with *DmPrtf1* and *DmPrpf39* depletion in flies.